Positron annihilation on single crystals of $YBa_2Cu_3O_{7-x}$

B. Barbiellini and P. Genoud
Département de Physique de la Matière Condensée, Université de Genève, 24 Quai E. Ansermet, CH-1211 Genève 4, Switzerland

J. Y. Henry
Centre de Etudes Nucléaires de Grenoble, Département de Recherche Fondamentale, 85 X, 38041 Grenoble CEDEX, France

L. Hoffmann, T. Jarlborg, and A. A. Manuel
Département de Physique de la Matière Condensée, Université de Genève, 24 Quai E. Ansermet, CH-1211 Genève 4, Switzerland

S. Massidda
IRRMA, PHB Ecublens, CH-1015 Lausanne, Switzerland

M. Peter and W. Sadowski
Département de Physique de la Matière Condensée, Université de Genève, 24 Quai E. Ansermet, CH-1211 Genève 4, Switzerland

H. J. Scheel
Institute of Micro- and Optoelectronics, Physics Department, Swiss Federal Institute of Technology, CH-1015 Lausanne, Switzerland

A. Shukla
Département de Physique de la Matière Condensée, Université de Genève, 24 Quai E. Ansermet, CH-1211 Genève 4, Switzerland

A. K. Singh
Physics Department, Harcourt Butler Technological Institute, Kanpur 208 002, Uttar Pradesh, India

E. Walker
Département de Physique de la Matière Condensée, Université de Genève, 24 Quai E. Ansermet, CH-1211 Genève 4, Switzerland
(Received 16 March 1990; revised manuscript received 10 September 1990)

We present lifetime and two-dimensional angular correlation of (positron) annihilation radiation (2D-ACAR) studies on $YBa_2Cu_3O_{7-x}$ single crystals, both on metallic and on insulating samples, in the hope of discriminating between band-structure and strong-interaction theories. Our measurements are discussed in the light of a large number of positron-annihilation investigations also made by other groups. Self-consistent band-structure calculations (linear muffin-tin orbitals and full-potential linear augmented plane waves) show that in the **k**-space-folded (001) projection we should see breaks from the cylindrical Fermi surface (FS) in the case of an ideal sample. Our experimental distributions suggest a smooth modulation (only to some extent described by the calculations) without sharp breaks, compromising a direct interpretation of the distributions in terms of FS topology. The 2D-ACAR technique cannot exclude the existence of the FS, since the trapping of positrons may occur in nonstoichiometric $YBa_2Cu_3O_{7-x}$ samples. However, it is to be noted that different samples measured by different groups are found to have similar momentum densities.

I. INTRODUCTION

The study of the high-T_c superconductors is attractive for many reasons. First discovered by Bednorz and Müller,[1] superconductivity in some perovskite cuprates mobilized scientists around the world, both to understand its origin and to find compounds with higher superconducting transition temperatures T_c. The broadest sources of information on the subject are the proceedings of the conferences held in Interlaken[2] and in Stanford.[3]

Positron annihilation has played an important role in the study of these new materials. Three techniques using positron annihilation are used in the study of the high-T_c superconductors.

First, *lifetime* measurements give information about positronic state and electronic densities, and are sensitive to sample defects, impurities, or phase transitions. Lifetime data are mainly used to characterize sample quality. For high-T_c superconductors, recent papers treat lifetime anomalies around T_c.[4–11]

Second, *Doppler-broadening* spectrometers measure the one-dimensional energy distribution of γ rays issued from annihilation. Data are directly related to the two-photon momentum distribution (TPMD) with, however, a low-momentum resolution, comparable to the Fermi momentum. On the other hand, the rapid detectors make this technique useful in time and temperature scanning measurements. An important feature characterizing

 ©1991 The American Physical Society

Doppler-broadening spectra is the shape parameter S. In high-T_c superconductors, a large scatter in the temperature-dependent results (reviews of Manuel[4] and Sundar *et al.*[12]) makes the interpretation difficult. The common point is that, around T_c, metallic samples show anomalies which are absent in the insulating sample.[13–16]

Finally, the *angular correlation of (positron) annihilation radiation* (ACAR) technique, described by Berko[17] and Mijnarends,[18] measures the TPMD, but with a momentum resolution better by 1 order of magnitude compared to Doppler broadening. In particular, two-dimensional (2D-ACAR) distributions, interpreted as once integrated TPMD, have shown fine details of the electronic structure in intermetallic compounds and alloys. The outstanding result is the extraction of the complex Fermi surface (FS) sheets from folded 2D-ACAR distributions. Earlier, we obtained a good agreement with linear muffin-tin orbitals (LMTO) band-structure calculations.[19–21] As of now, more sophisticated band-calculation methods like full-potential linear augmented plane waves[22,23] (FLAPW) and Korringa-Kohn-Rostoker[24] (KKR) are available for the calculation of theoretical 2D-ACAR in $YBa_2Cu_3O_{7-x}$. This technique was applied by several groups, including ours, for the study of superconducting oxides. The ACAR technique has the advantage of directly measuring the momentum distribution whereas de Haas–van Alphen and Shubnikov–de Haas methods are inefficient for materials where electronic mean free paths are smaller than the cyclotron radius.

Several measurements have been carried out both on insulating and metallic single-crystal oxides using the 2D-ACAR technique in order to investigate and to compare their electronic structure, and in particular in the search to see the FS. Unfortunately, as things stand, with positron annihilation one cannot determine the existence of a FS since 2D-ACAR data have been interpreted differently with contradictory conclusions. Data obtained on the La_2CuO_4 insulator[25,26] are well described by a model derived from a linear combination of atomic orbitals-molecular orbital (LCAO-MO) scheme as developed by Chiba,[27] excluding the dominance of FS signals in the distributions. On the other hand, Tanigawa *et al.*[28] interpret their data on the same compound in terms of FS topology. Smedskjear *et al.*[29] and Bansil *et al.*[30] deduce the existence of four FS sheets from their data measured on the metallic compound $YBa_2Cu_3O_{7-x}$. In the past we made similar claims,[31] but investigations on the insulating $YBa_2Cu_3O_{7-x}$ compound, according to Peter's suggestion, revealed structures similar to the metallic one. Thus, the principal structures seen in $YBa_2Cu_3O_{7-x}$ data reflect other origins[32] and our previous interpretation of positron-annihilation data has had to be revised.

In order to clarify the present situation of positron annihilation on $YBa_2Cu_3O_{7-x}$, we will detail in this paper our experimental results, measured on both metallic and insulating $YBa_2Cu_3O_{7-x}$ compounds. These will be compared with two different theoretical calculations. The first, performed in the independent-particle model (IPM) from LMTO and the second with FLAPW methods.

II. EXPERIMENTAL AND CALCULATION DETAILS

A. Preparation and characterization of samples

Each sample will be identified as follows: *SPhkl*, where *S* is the sample name (*A*, *B*, or *C*), *P* identifies the phase (*I* for insulating, *M* for metallic) and *h*, *k*, and *l* are the Miller indices of the measured plane. The phase is not specified when both the metallic and insulating phases are implied.

Our first 2D-ACAR measurements on $YBa_2Cu_3O_{7-x}$ were performed on small metallic single crystals prepared by Damento *et al.*[33] Results on this sample have already been reported.[31,34–37]

Later, some larger single crystals of $YBa_2Cu_3O_{7-x}$ were prepared by Sadowski and Scheel[38] from a high-temperature solution using the CuO–28% BaO eutectic as a solvent. The insulating phase was obtained after annealing under argon pressure and the semiconductorlike behavior of the resistivity was confirmed. A proper heat treatment under oxygen pressure gave superconducting twinned single crystals. The crystals are platelike, typically 10 mm^2 in the a/b plane, with a maximum thickness of 1.5 mm along the c axis. Scanning electron microscope investigations reveal an undetermined quantity of flux still embedded in the crystals. Measurements in the (110) plane have been carried out on the same single crystal of about $3\times5\times0.1$ mm^3, both in the insulating (sample *AI*110) and in the metallic phase (sample *AM*110). *AM*110 showed two resistive transitions at 57 and 63 K. The midpoint of the inductively measured transition is at 57 K with a width (10–90 %) of 5 K. This relatively low value of T_c is attributed to aluminum impurities (about 6 at. %, Y+Ba+Cu+Al=100 at. %) coming from the crucible. No degradation was observed inductively after 2D-ACAR measurements. Lifetime measurements showed a single component at 215 and 192–185 ps, respectively, for samples *AI*110 and *AM*110. The latter lifetime range comes from different fits. The statistical error on all our lifetime results are estimated to be ±2 ps.

We also measured a large sample of $11\times2.4\times0.7$ mm^3 size, grown by Henry,[39] presenting good superconducting properties in the metallic phase: $T_c=90$ K and δT_c (90–10 %)=1 K. This sample contains 7% by weight of green phase Y_2BaCuO_5. It was measured in the (110) plane (*BM*110). After a 4-day heat treatment, the same sample became insulating and tetragonal with an O concentration between 6.08 and 6.12 and was measured for the same orientation (*BI*110).

Finally, we measured a third sample (prepared in the same manner as *A*110) in the (001) plane. To get a sufficiently high counting rate we aligned five single crystals together on a copper sample holder. This was done both for a set of insulating (*CI*001) and for a set of metallic (*CM*001) single crystals (all of them coming from the same melt). The orientation was achieved within ±2.5° using an x-ray Laue diffractometer. The large size of samples *CI*001 and *CM*001 in the a/b plane ($\sim4\times4$ mm^2) guaranteed the absence of positron annihilation in the sample holder. The inductively measured T_c value before and after 2D-ACAR measurements of sample

TABLE I. Characteristics of the samples and crystallographic planes of 2D-ACAR measurements.

Sample	Origin	Shape	Sizes (mm^3)	Positron lifetime (ps) at 300 K	T_c (δT_c)	O concentration/ impurity (%)	Plane
*AI*110	Sadowski	thin	3×5×0.1	215	insulating	<6.2/6% Al	(110)
*AM*110	and Scheel[a]	plates		192–195	57 K (5 K)	6.6–6.8/6% Al	
*BI*110	Rossat-	bulk	11×2.4×0.7		insulating	6.08–6.12/7% Y_2BaCuO_5	(110)
*BM*110	Mignod *et al.*[b]				90 K (1 K)	>6.9/7% Y_2BaCuO_5	
*CI*001	Sadowski	thick	3×3×1.5	215–219	insulating	<6.2	(001)
*CM*001	and Scheel[a]	plates		180–184	80 K (4 K)	>6.8	

[a]Reference 38.
[b]Reference 39.

*CM*001 was 80 K with a width of 4 K, suggesting no degradation during measurments. The Meissner effect was measured on two of the *CM*001 crystals, showing 8.7% and 15 % ratios. X-ray powder diffraction showed traces of $BaCuO_{2-x}$ and CuO, but no green phase was observed. Lifetime results showed single components of 215–219 and 180–184 ps, respectively, for samples *CI*001 and *CM*001.

All metallic samples used for 2D-ACAR measurements were twinned. The characteristics of all measured samples are summarized in Table I.

B. Measurements

Our experimental setup has been described by Bisson *et al.*[40] Some modifications have been made since then. (1) We use a liquid-helium cryostat offering a wider range of temperatures (1.8 to 800 K) with low consumption. (2) Two *J*11 microprocessors [from Digital Equipment Corporation (DEC)] perform the data acquisition at a maximum rate of 1000 events/s. (3) The sensitive area of the γ-ray detectors (high-density proportional chambers) is now 30×30 cm^2.

Measurements were performed under vacuum ($<10^{-6}$ Torr) using a 25-mCi ^{22}Na positron source, and a magnetic field of 2T to focus the positrons on the sample. The data acquisition rate varied between 60 to 200 events/s, depending on the sample geometry and source intensity. The global measuring time amounts to 14 months. The detector-sample distance was 7.72 m. We chose 0.15 mrad/bin as the mesh of the histogram, covering a momentum space of $(-30\ +30\ \text{mrad})^2$. The angular resolution full width at half maximum (FWHM) taking only geometrical considerations into account is about 0.3×0.5 $mrad^2$ (the width of the samples is responsible for the value 0.5). The thermal effects on the positron also contribute to a broadening of the resolution function with the temperature-dependent Boltzmann (Gaussian-like) distribution. The estimated resolution for the spectra of *CI*001 and *CM*001 measured at 40 K is 0.5×0.6 $mrad^2$.

In order to make a detailed analysis of the 2D-ACAR structures, we opted for distributions with large statistics. *AI*110 and *AM*110 were measured at 10 K with 1.2×10^8 events. More than 2.1×10^8 events were obtained on *CI*001 and *CM*001 at 40 K, 1.7×10^8 events on *BM*110 at 83 K (superconducting state) and 93 K (normal state). *BI*110 was measured at 37 K, with statistics of 1.6×10^8.

To study the temperature dependence of the shape parameter *S*, statistics of $1-3\times10^7$ have been accumulated for temperatures spaced by 20 K. *AI*110 and *AM*110 were measured from 30 to 150 K, *BI*110 from 37 to 180 K and *BM*110 from 11 to 303 K.

Our lifetime measurements reported in Table I were obtained using a standard fast-fast spectrometer similar to that described by Bedwell *et al.*[41] The source was sandwiched between two pieces of the sample when available, or between the sample and an annealed Fe sample with a well-determined lifetime, when only one piece was available. All measurements were made at room temperature and followed by the ACAR measurements. The spectra were analysed using the POSFIT analysis program.[42] The resolution was found to be 210 ps for a ^{60}Co source and symmetric discriminator windows, and about 260 ps as determined by POSFIT after analysis of the spectra. A thin aluminium foil was used as a support for the source and a source correction of 5–6 % was made. Each spectrum contains a total of about 700 000 counts.

C. Data analysis of 2D-ACAR

The raw measured 2D-ACAR histograms have been corrected with the experimental angular efficiency histogram, evaluated for each measured 2D-ACAR spectrum on a set of 10^9 anticoincident events. In order to study the shape of our spectra, we consider a central slice (2-mrad thick) cut through the 2D-ACAR spectrum and define a shape parameter *S* as the ratio of the central area (within ±3.6 mrad) by the total area of the slice. Generally the choice of the central area is left to the author and makes comparison of absolute values between different laboratories impossible. However, the evolution of the *S* parameter with temperature may be compared with other such results (Doppler broadening and ACAR).

In order to exhibit the small anisotropies of the 2D-ACAR distributions, we have subtracted the part of the distributions which is invariant to rotations; this isotropic part, which is calculated for each *p* radius as the

mean value of the 2D-ACAR, has been smoothed before subtraction. Some authors prefer to calculate the isotropic part using the minimum value of the spectrum for each p radius so that all anisotropic structures are positive. This latter procedure was used by Smedskjaer *et al.*[29]

The Lock, Crisp, and West[43] (LCW) folding of spectra is a procedure which reinforces FS-related structures by constructive interference and reduces noise by destructive interference. The LCW distributions may be interpreted in terms of 2D projections of the occupation number in the crystal **k** space (LCW theorem), giving direct access to the FS topology. However the LCW theorem is valid only if the following two conditions are fulfilled: the modulation of the positron wave function and of the annihilation enhancement factor must be negligible. In this ideal case, the occupied electronic states make a contribution equal to unity of the 2D **k**-space LCW distribution while the empty states give no contribution. Therefore, the fully occupied bands give a constant contribution to the folded distribution, and the partially filled bands produce an image of the projected FS. In materials with a large number of filled bands, like $YBa_2Cu_3O_{7-x}$ the FS signal from the partially filled bands is small compared to the constant contribution from the occupied states. In fact, the positron wave function changes the weight of the occupied states in **k** space. Hence, the FS signal may be masked by the distortion induced by the filled-band states, especially if their number is large. Moreover, an insulator can show a nonconstant LCW.

Twinning in the metallic crystals leads to another approximation which may affect the LCW-folded data: if one supposes an equal contribution of both domains, a tetragonal symmetric spectrum should result due to the superposition of the contribution from each domain. In the analysis, a mean lattice parameter is used for a and b and is equal to 3.86 Å, $c = 11.63$ Å. But the relatively small orthorhombic distortion of the metallic twinned single crystals will not affect our results, because the difference in length of the $2\pi/a$ and $2\pi/b$ sides of the Brillouin zone (BZ) lies within the experimental resolution.

D. Calculation procedure

The TPMD calculations reported here were performed using LMTO and FLAPW methods. Other TPMD band calculations were performed by Bansil *et al.*,[24] Massidda,[22] and Singh *et al.*[23] As concerns the band calculations, LMTO and FLAPW are in good agreement. As predicted by the LCW theorem, this agreement persists [Fig. 2(c) of Refs. 32 and 44 and Fig. 1 of Ref. 24) for a constant positron wave function. For a nonconstant positron wave function, the agreement between our previous LMTO calculations[32] and FLAPW (Ref. 23) broke down because of an error in the positron amplitude data in the atomic spheres. However, our calculated positron densities[44,45] were correct. We present here our TPMD results.

For the LMTO self-consistent calculations, the electronic structures are calculated on 192 **k** points in the orthorhombic irreducible BZ. The band-structure results and details of the calculation for the $YBaCuO_7$ compound have been given earlier.[46] For $YBaCuO_6$ we use the same structural data as for $YBaCuO_7$ but the O(1) site is replaced by an empty sphere of equal size. The self-consistent non-spin-polarized band structure is metallic and the insulating case is modeled within the resulting bands by a full occupation of the otherwise partially occupied last bands. This is equivalent to saying that the Fermi energy (E_F) is raised and varies with **k** in order to fall within the gap region at slightly higher energy. This procedure is likely to change the details of the results compared to the case of the actual antiferromagnetic insulating phase (which is not stable in local-density calculations). Also, the real structure has slightly different atomic positions and is tetragonal while we keep the orthorhombic structure facilitating the comparison with the metallic phase. The total valence contribution is obtained from two self-consistent band calculations both in $YBaCuO_6$ and $YBaCuO_7$. The contributions from the low-lying semicore Y 4p, Ba 5s are obtained from a calculation in which these five bands are included in the valence. Contributions from all other bands including semicore Ba 5p are taken from the calculations in which Y 4p and Ba 5s are taken as core states renormalized over the Wigner-Seitz (WS) spheres. This is motivated by the fact that there is a considerable overlap of the positron wave function with these states. In this way it is possible to include Y 4p and 5p and Ba 5s and 6s states despite the very wide valence region of 2.5 Ry. The positron states are determined using the potential from the latter (i.e, high-core states) calculations, but they are fairly insensitive to this choice.

In $YBaCuO_7$ we obtain an E_F at 0.334 Ry, while in the momentum density [$\rho(\mathbf{p})$] calculations we use 0.35 Ry. This is done in order to fully occupy a flat band near E_F along Γ to X as in the FLAPW calculation of Massidda *et al.*[47] and Yu *et al.*[48] In this context it should be mentioned that fine details of the band structure are not as precisely determined as in the FLAPW calculations, largely because we have not tried to optimize the WS sphere radii. However, we can calculate a larger number of **k** points due to the efficiency of the LMTO method and we can obtain a similar FS topology by shifting E_F. The Γ point in LMTO is not exactly at (0,0,0) but near it, which has introduced some instability of certain characteristics of the wave functions at this point.

The positron potential was calculated by inverting the Coulomb potential and adding a local-density-approximation (LDA) positron-electron correlation potential as suggested by Boronski and Nieminen.[49] Only the s part of the positron state is included in the calculations of matrix elements. The correction of the atomic sphere overlap[50] was taken into account, but the number of reciprocal-lattice vectors needed for this correction is quite limited (755) for the large number of sites in the YBaCuO unit cell. We can then obtain $\rho(\mathbf{p})$, the TPMD for positron annihilation or the electron momentum density (EMD) for Compton profiles. Except when specified, the calculations presented here are performed in the independent-particle-model (IPM) approximation.

Calculated LCW distributions are to be compared with experiments only after superposition of **x** and **y** directions in the metallic case since real crystals are twinned. Additional broadening is introduced in order to take experimental resolution into account.

As for FLAPW calculations, they start from the band structure[47,48] and are described in detail by Massidda *et al.*[22] We will just mention here that we calculated the positron wave function of $YBaCuO_7$ including both an electron-positron LDA correlation potential[49] and an electron-positron annihilation enhancement following the suggestion of Jarlborg and Singh.[51] The contribution of the core level, which is rather small according the LMTO calculations, was not included, but the outermost Y and Ba semicore *p* electrons were included in the valence band. The *s* and *p* parts of the positron state were included in the calculations of matrix elements.

III. RESULTS AND DISCUSSION

A. Positron lifetimes

Lifetime measurements indicate essentially a single component in all samples. The lifetime for the insulating, tetragonal crystals (215–220 ps) is longer than that measured for metallic, orthogonal crystal (180–195 ps). How do these figures compare with other measurements and calculations? Calculations find an increase in lifetime for the insulating state with respect to the metallic state. Bharati *et al.*[52] calculate a lifetime of 190 ps for $YBaCuO_7$ increasing to 220 ps for $YBaCuO_{6.5}$ and 234 ps for $YBaCuO_6$. They argue that this increase is due to different ordered arrangements of vacancies in the different phases. Jensen *et al.*[53] calculate a bulk lifetime of 159 ps for $YBaCuO_7$, increasing to about 175 ps in $YBaCuO_{6.5}$ and 207 ps in $YBaCuO_6$. They find that the oxygen vacancy is a shallow trap and can only very weakly localize the positron. On the other hand, the metallic vacancies are strong traps and the lifetimes corresponding to trapping in isolated vacancies are: 207 ps for Cu(1), 182 ps for Cu(2), and 206 ps for Y. According to these authors the scatter in different measurements reflects the varying influence of weak and strong vacancies in different samples. They propose that the measured lifetimes for single crystal $YBa_2Cu_3O_{7-x}$, which are greater than calculated values, are due, at least in part, to trapping. As for measured lifetimes in single crystals, Harshmann *et al.*[9] found 176 ps, Sundar *et al.*[12] find 190 ps in $YBaCuO_7$, and Moser *et al.*[6] find 176 ps in $YBaCuO_{6.5}$. Corbel *et al.*[8] measure lifetimes in ceramics and identified, in particular an annihilation state corresponding to a lifetime of 190 ps. They propose that this lifetime corresponds to a defect which is identified with oxygen-deficient regions. They obtained a single lifetime component for some of their samples which they attributed to positron saturation in a defect corresponding to the observed lifetime, rather than the absence of defects. Moser *et al.*[6] studied the effect of irradiation on samples. The irradiation induced defects increased lifetimes by 10 to 50 ps. It is to be remarked that impurities can also alter the bulk lifetime. Zinc impurities are known to decrease lifetime and gallium impurities to increase it in $YBaCuO_7$ at room temperature.[11]

The above considerations imply that increase in lifetimes due to trapping is not substantial and it is, in general, impossible to resolve different lifetime components corresponding, respectively, to annihilation in the crystal bulk and in defects. The single lifetime component observed therefore cannot rule out trapping since it would well represent an average value for two or more components grouped closely together.

B. 2D-ACAR distributions

Let us first compare the 2D-ACAR spectra measured in the insulating and in the metallic phase. Figure 1 shows lines through the 2D-ACAR's normalized to the same volume, along different directions. We observe an evident difference between the metallic and insulating spectra; both in the (110) and in the (001) planes, we observe a significant narrowing of the 2D-ACAR for the insulating state. This narrowing has also been observed by von Stetten *et al.*[16] in polycrystalline samples. The ratio of the magnitudes of the insulating and metallic spectra is similar (within 3%) for *A*110 and *B*110. However, the absolute magnitudes are about 10% smaller in *B*110 compared to *A*110. This indicates that results obtained are sensitive to the sample quality and method of preparation (see Secs. II A and III B). The difference in magnitudes between the spectra of *CI*001 and *CM*001 is significant (a factor 2) indicating that the [001] orientation is more adequate for such observations.

Figure 1 illustrates the difference between the metallic and insulating spectra, which is large around zero momentum and small for higher momenta. We used this observation to make the qualitative analysis presented in Fig. 2, which shows the contour plots of the difference between metallic and insulating spectra. These were previously treated so as to superpose the high-momentum parts which are very similar for both phases. In the (001) plane, the difference is sizable only within the first BZ [Fig. 2(c)]. This difference may be explained by the more delocalized (real-space) annihilation in the $YBaCuO_6$ compound, which contains oxygen vacancies located along the so-called fencelike region. As calculated earlier,[16,22,45,54] the positron samples primarily this region. In the (110) plane, the two phases show differences over a much larger region along the [001] direction [Figs. 2(a) and 2(b)], and this may be interpreted as the localization of electrons in the (001) plane.

The comparison of calculated and experimental 2D-ACAR distributions shows that the electron-positron correlation effects are rather important. We see from Fig. 3, which exhibits a line extracted along [100] from the metallic spectra in the **c** plane, that the **p** localization is higher in the experiment than in the IPM calculation. Many theories exist for enhancement, at least in metallic systems[51,55,56] and it is known that the inclusion of an enhancement factor reflecting the electron-positron attraction can produce a narrowing of the calculated profile. In order to get a qualitative picture of the influence of these electron-positron correlation effects on

the theoretical distributions, we have calculated a 2D-ACAR distribution of the metallic phase including the electron-positron correlation effects using the scheme proposed by Jarlborg and Singh.[51] Moreover, we have considered an electron-positron correlation potential[49] in the Schrödinger equation for the positron. In this case the positron wave function localizes more in the high-electron-density region, producing an opposite effect to that of the enhancement factor. However, the final result is still narrower than the IPM as shown in Fig. 3. Similar trends have been observed by Massidda[22] in his FLAPW calculations. The effects of enhancement in the insulating case are uncertain. For this reason we will compare the $YBaCuO_7$ and $YBaCuO_6$ distributions calculated in the IPM only.

An important question is the following: Are Fermi breaks observed in the 2D-ACAR from metallic samples? Bansil *et al.*[30] analysed the structure of the 2D-ACAR derivative lines and give an affirmative answer. Haghighi *et al.*[57] also studied the derivatives but they do not find any structures indicating boundaries between electronic occupied and unoccupied regions. We have made a similar analysis shown in Fig. 4. We came to the same conclusion, namely, that Fermi breaks, if they exist in metallic samples, are too small to be observed with the current statistics. However, the metallic case (dotted lines) is similar to the result of Hgahighi *et al.*[57] More precisely, the behavior of their lines seems to lie between our metallic and insulating line behavior. This may be explained by a little loss of oxygen in their samples, as suggested by the authors, giving a tendency to insulating behavior.

We have also measured the evolution of the 2D-ACAR shape parameter S (described above) with temperature. Earlier measurements[34] showed an erroneous behavior for $S(T)$ due to the contribution of the vacuum grease used to glue the crystals. Similar measurements were made by von Stetten *et al.*[58] leading to the same conclusion. The reviews made by Manuel[4] and Sundar

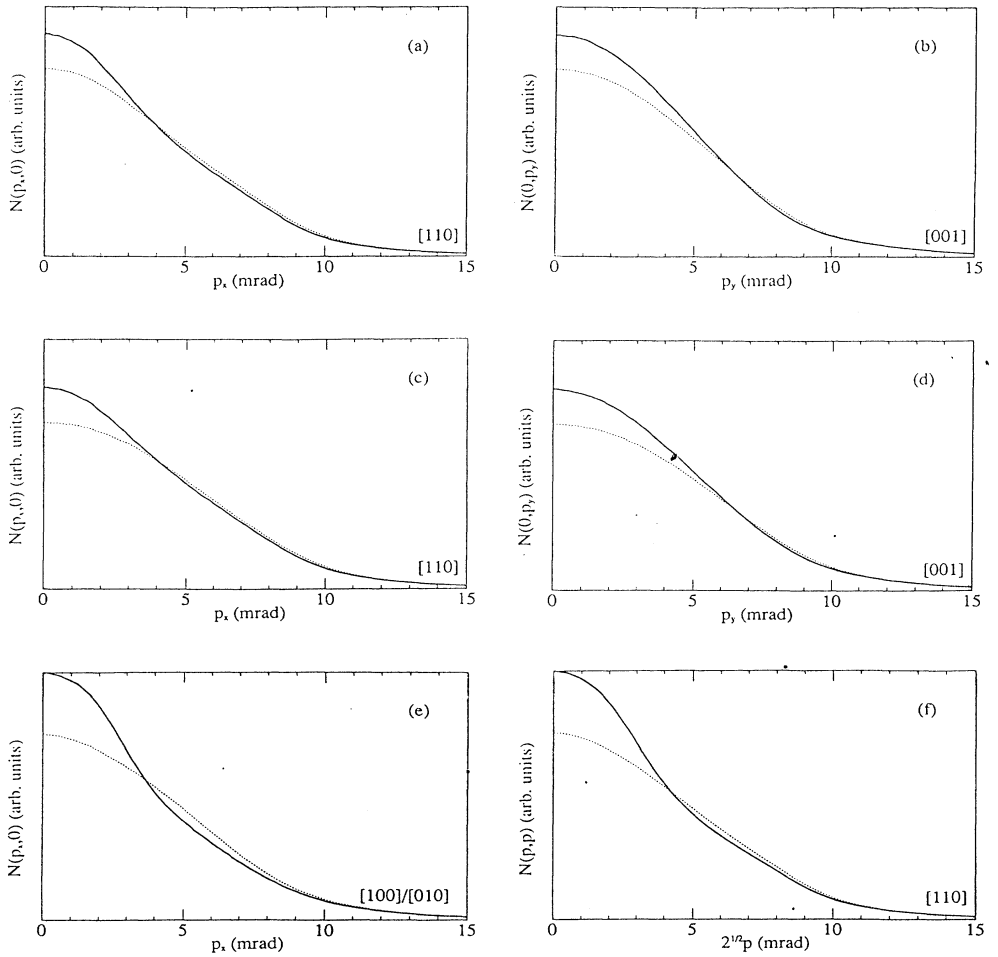

FIG. 1. Lines extracted from the (a)–(d) (110) and (e) and (f) (001) 2D-ACAR distributions from a $YBa_2Cu_3O_{7-x}$ single crystal, both in insulating (solid lines) and metallic (dashed lines) phases. The distributions have been smoothed by a square function of 0.75 mrad side. The total width of the line is 1.5 mrad. (a) Sample $A110$, [110] line. (b) Sample $A110$, [001] line. (c) Sample $B110$, [110] line. (d) Sample $B110$ [001] line. (e) Sample $C001$ [100]/[010] line. (f) Sample $C001$, [110] line. All distributions have been normalized to the same volume. All ordinates are in the same arbitrary units.

et al.[12] present the large variety in the temperature-dependent behavior of S making any clear interpretation difficult. However, there is a consensus about the difference between metallic and insulating samples: only metallic samples present an anomaly of S at temperatures comparable to T_c. From our 2D-ACAR data, we have measured the S parameter of samples $BI110$ and $BM110$ [Figs. 5(a) and 5(b), respectively]. When compared to the results of others authors (see review paper quoted above), the modulation of the curves agrees best with that observed by von Stetten *et al.*[16] for their polycrystalline samples Dns and Bs: in the insulating phase, S varies linearly and does not show any significant anomaly around T_c. However, the metallic phase shows clearly a sharp change of slope between 100 and 125 K. These authors give different possible explanations such as correlation effects, structural changes below T_c, and changes in positron trapping probability.

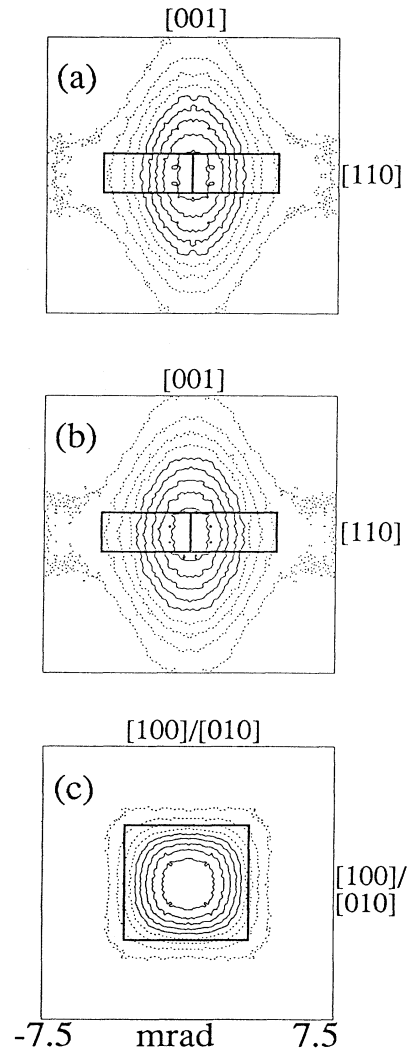

FIG. 2. Contour levels of the difference between insulating and metallic 2D-ACAR spectra measured in sample (a) $A110$, (b) $B110$, and (c) $C001$. The spacing between levels is 10% of the total magnitude. The upper levels are drawn with the solid lines. The right-angled solid line shows the first BZ. The zero momentum is at the center in the figures. The data has been folded according to the symmetry.

C. Anisotropies

If we presume that the contribution of trapped positrons is isotropic, then in considering the anisotropic part of 2D-ACAR distributions, we have a quantity which is free of a possible contribution from positrons trapped in defects. We may therefore attribute the observed anisotropies to the electronic structure only, since the isotropic part is featureless. No anisotropic contribution from trapped positrons has yet been observed. The neutron-irradiated Al compared to well-annealed Al does not show any additional anisotropic structures,[59] but the anisotropic effect due to the prevacancies in Cd is not really understood.[60] We cannot exclude an eventual anisotropic contribution from the defects in $YBa_2Cu_3O_{7-x}$ and this problem needs more investigation.

The isotropic part of experimental 2D-ACAR has been subtracted (as described in Sec. II C), giving rise to structures shown in Figs. 6(a) ($AM110$, $AI110$), Fig. 6(b) ($BM110$, $BI110$), and 6(c) ($CM001$, $CI001$). They all exhibit the characteristic symmetry of the measured plane.

We can now compare the ratio of the maximum amplitude of the anisotropic part of the 2D-ACAR to the maximum amplitude of the original 2D-ACAR, a quantity which we call r_{ANIS}. For $AI110$, $r_{\mathrm{ANIS}}=12\%$ and for $AM110$, $r_{\mathrm{ANIS}}=6\%$. For $BI110$ and $BM110$ these values are, respectively, 8.8 and 2.3 %. As discussed earlier, these discrepancies are due to differences in sample quality and growing methods. Effectively, $A110$ contains traces of Al and shows two resistive transitions, while $B110$ is contaminated by the green phase. The r_{ANIS} deduced from the calculated TPMD is about 6% for both metallic and insulating phase. The agreement is good for the metallic phase, whereas the disagreement for the insulator could be explained by the approximations used for calculating the electronic structure. For comparison, these values for r_{ANIS} generally exceed those obtained in $A15$ structure compounds[61–63] (1.5–6 %). For $CI001$ and $CM001$, we find for r_{ANIS}, respectively, 3.5 and 3.7 %, comparable to that measured by Smedskjaer *et al.*[29] (3%) in the sample plane. The 2D character of the electronic structure, in particular, the weak localization of electrons in the (001) plane compared to the strong one along [001], may explain the small anisotropic values in the (001) plane compared to those measured when integrating along [110].

If we analyze the anisotropic structures of $CM001$ in more detail [Fig. 6(c), left], we observe a peak indicating a high-momentum component (HMC) centered in the neighboring BZ (110), compensated by the valleys along the [100]/[010] axis. These structures are largely the same as those obtained by Haghighi *et al.*[57] in the (001) plane. These authors extract the measured anisotropic part in the same way as we do, and they reproduce this feature by a simple calculation using a cluster made of a Cu atom in a Cu-O chain surrounded by four O atoms.

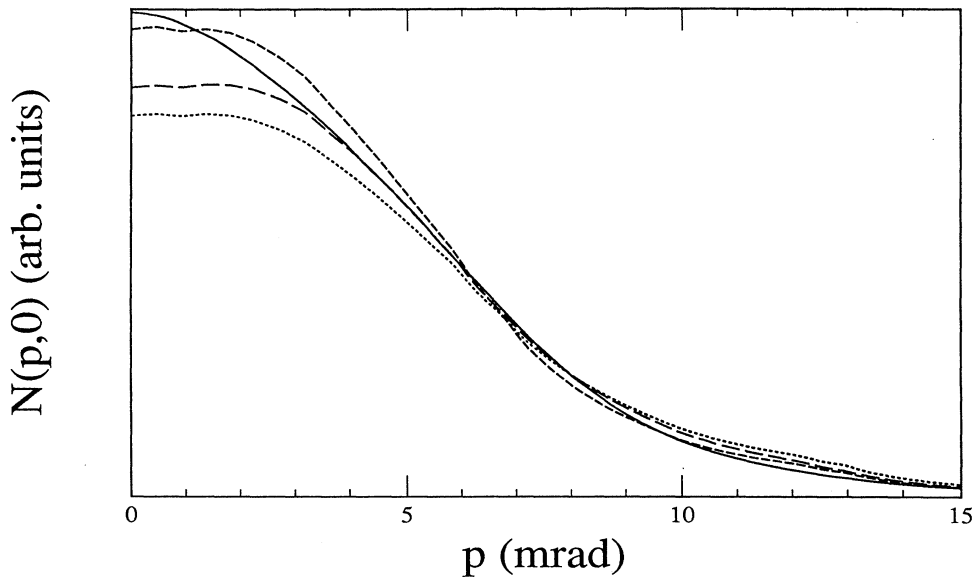

FIG. 3. [100] lines extracted from the (001) plane 2D-ACAR of the metallic phase. The experiment (solid line) is presented together with calculations obtained in the IPM approximation (dotted line), including an enhancement factor for matrix elements (dashed) and including an electron-positron correlation potential (long-dashed). The calculated distributions are normalized to the corresponding experimental volume.

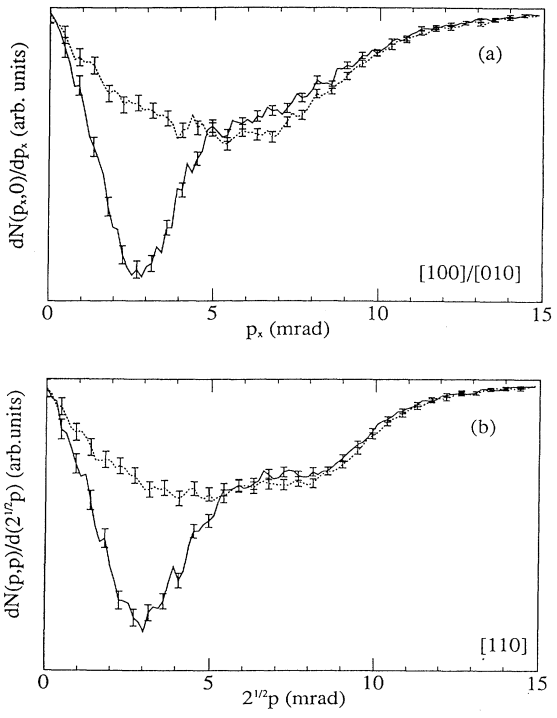

FIG. 4. Derivative of the (a) Γ/Z-X/Y line and (b) Γ/Z-R/S line, extracted from the distributions measured in the insulating sample *CI*001 (solid line) and the metallic sample *CM*001 (dotted line). The distributions have been normalized to the same volume, and smoothed by a square function of 0.45 mrad side. Both ordinates have the same scale. The error bars are based on the statistics of the raw ACAR, and are shown for every third channel.

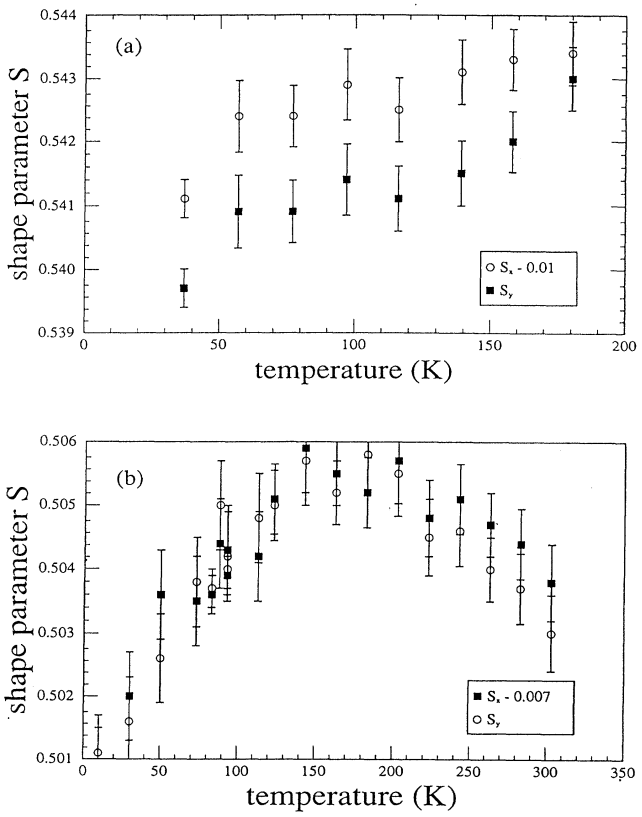

FIG. 5. Evolution of the shape parameter S with temperature, measured in the insulating (a) *BI*110 and (b) *BM*110 samples. Open circles: S_x along the [110] direction; solid squares: S_y along the [001] direction. S_x has been shifted by (a) -0.01 and by (b) -0.007, in order to use the same scale for S_x and S_y.

Between isulating and metallic phases, the differences are significant only for the (001) projection. The anisotropic part of our calculated 2D-ACAR's [Fig. 6(d)] shows similarities with the experimental ones, especially for the metallic phase. The calculated and experimental structures appear at the same positions, while Haghighi *et al.*[57] are not able to obtain this agreement. The observed structures in the calculations without taking into account the positron wave function (not shown) are very similar. This suggests that, in **p** space, the 2D-ACAR anisotropy is mainly due to electronic structures.

D. LCW distributions and FS studies

It is well established that any FS gives rise to discontinuities in the TPMD, and thus also in the 2D-ACAR if measured in the proper plane. For instance, in alkali metals the 2D-ACAR shows a nearly spherical FS, the radius of which gives the Fermi momentum. In transition metals or intermetallic compounds, the Bloch electrons are no more free, and the breaks induced by the Fermi electrons are spread over a large momentum domain. Not only the conduction electrons but also the core electrons are sampled by positrons giving rise to a non-negligible Gaussian-shaped contribution. The shape of a Fermi break in an ACAR spectrum depends on how the hole or electron pockets are projected onto the measured plane, and may be steplike in the case of a cylindrical FS. In $YBa_2CuO_3O_{7-x}$ in particular, the (001) plane should reveal sharp discontinuities of the FS as predicted by band-structure calculations.[48] The low dispersion bands calculated along the c axis lead to a quasi-2D sys-

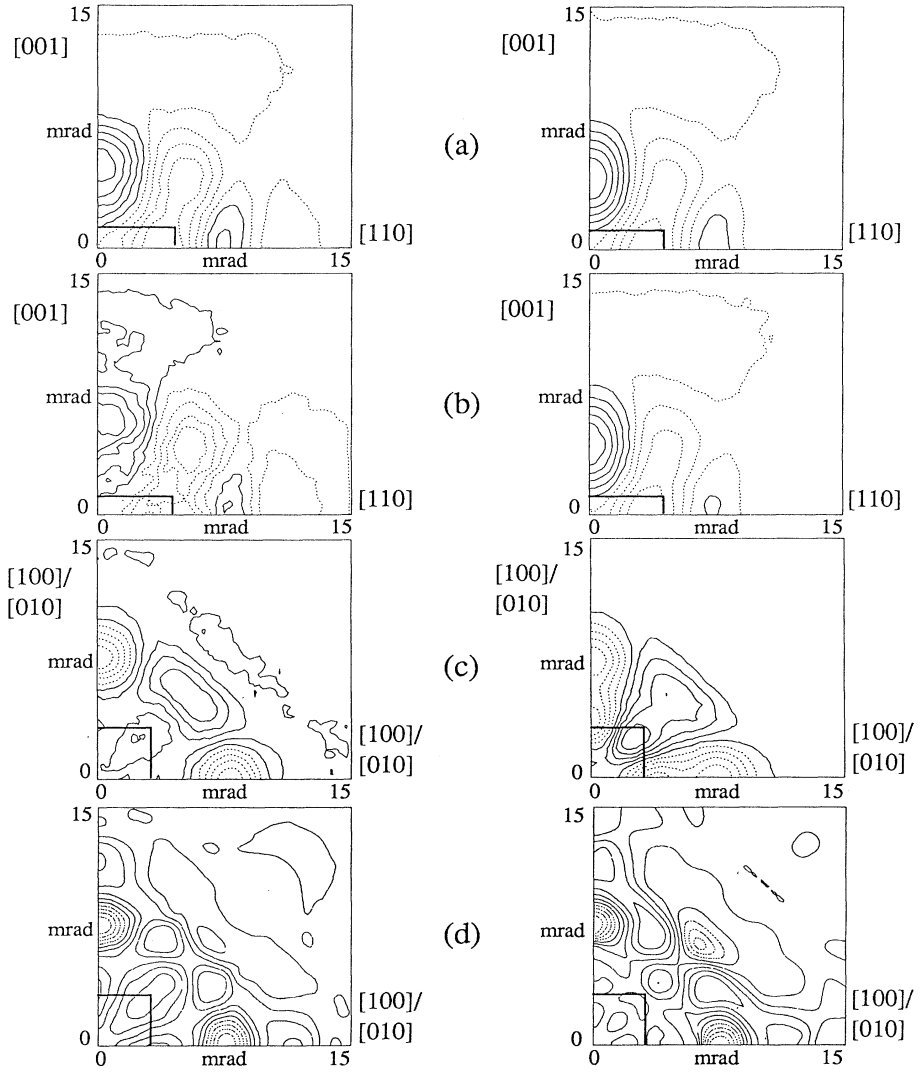

FIG. 6. Contour levels of a fourth of the anisotropic part of the 2D-ACAR spectra (the zero momentum is at the left bottom corner). The data have been folded and smoothed by a square function of 0.75 mrad side. Left column: metallic phase; right column: insulating phase. (a) Sample $A110$, (b) Sample $B110$, (c) Sample $C001$, (d) Twinned TPMD calculations. The spacing between levels is 10% of the total anisotropic magnitude, the upper levels are drawn with the solid lines. The right-angled solid line shows the first BZ.

tem, giving rise to cylinderlike FS sheets.

Figure 7 illustrates the LCW-folded distributions for samples $A110$, $B110$, and $C001$. The data has been smoothed by a square function of sides=0.45 mrad, which is close to the angular resolution of the measured data. Only one of three nodes of the drawn net is an independent point. We shall now discuss Fig. 7(e), ($CM001$), which can be directly compared to results obtained by other authors.[29,57,64] It shows a smooth distribution. Sharp structures, which could have signaled the presence of a FS, are absent. This is compatible with the results of Haghighi *et al.*[57] We also reproduce the general trends observed by Smedskjear *et al.*[29] However, our distributions are much smoother, probably because we have statistics which are 50 times greater. Earlier, we presented a distribution showing some structure on the Γ/Z-X/Y line.[32] This, however, disappeared when a careful examination of the unsymmetric part of the 2D-ACAR spectrum suggested a rotational correction of 2° (the precision on the orientation of the mounted samples is ±2.5°). We had also interpreted measured (100), (110), and (210) plane LCW distributions as evidence of a FS.[31] This was before having investigated the (001) plane and having measured 2D-ACAR of the insulating sample $CI001$ [Fig. 7(f)]. Surprisingly, the magnitude of the LCW modulation of the insulating phase is more than twice that of the metallic phase. This is further discussed in Fig. 9. The interpretation of the measurements in the (110) plane is more difficult, since the difference between the metallic [Figs. 7(a) and (c)] and insulating [Figs. 7(b) and (d)] spectra is not statistically significant.

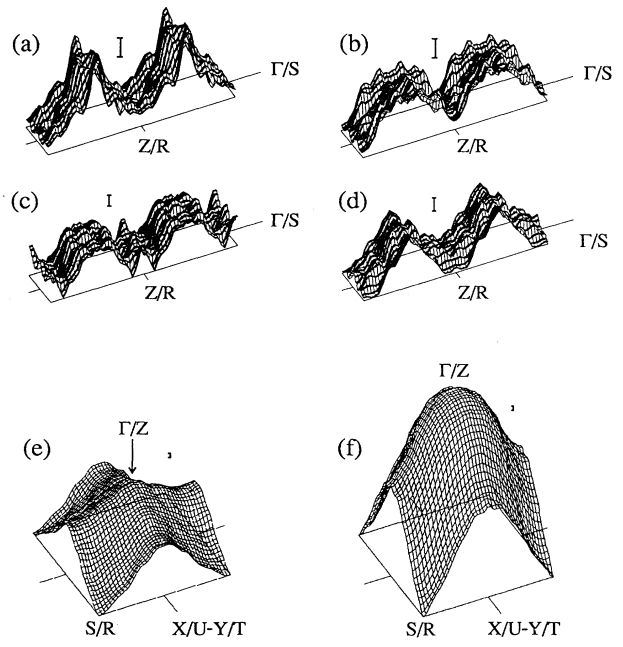

FIG. 7. LCW-folded 2D-ACAR distributions. The data have been smoothed by a square function of 0.45 mrad side. Left column: metallic phase; right column: insulating phase. (a) and (b) Sample $A110$, (c) and (d) Sample $B110$, (e) and (f) Sample $C001$. The magnitude of the LCW signals are comparable since the 2D-ACAR have been normalized to the same volume before LCW folding. Only the nonconstant part of each distribution is shown. The error bars are based on the statistic of the raw ACAR and of the efficiency function.

Figure 8 presents a line along Γ/Z-S/R extracted from the non-constant part of the LCW distribution shown in Fig. 7(e). To compare our results with the corresponding one of Smedskjaer *et al.*[29], we also present the same line (solid) extracted from the LCW-folded anisotropic part of the 2D-ACAR. The decline from Γ/Z to S/R is reproduced in both cases, but the small features seen by Smedskjaer *et al.* and interpreted as Fermi breaks cannot be deduced from our results if we take into account the error bars. In order to characterize the observation of a small signal, we can use a statistical test, for example, the Kolmogorov-Smirnov test,[65] which compares the distribution of the set of points defining the measured signal with that of an expected model. The test accepts (or rejects) within a given confidence interval

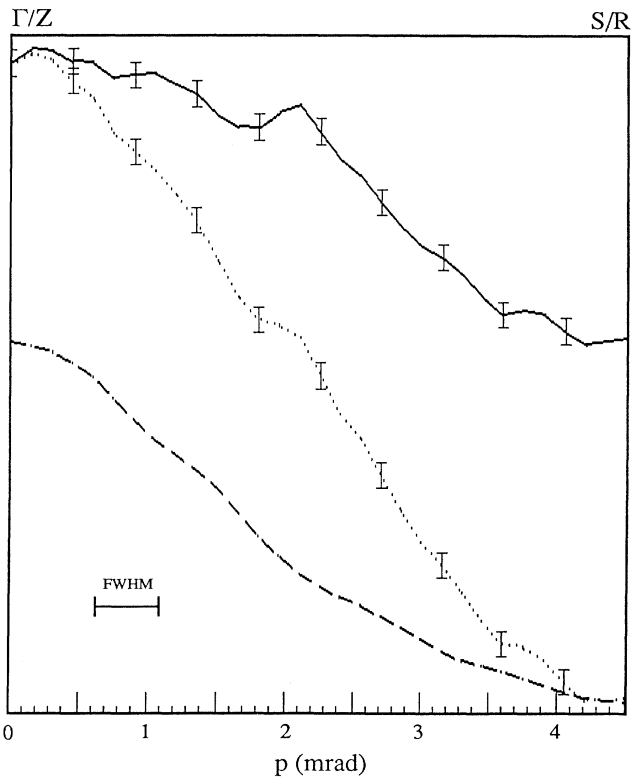

FIG. 8. Lines extracted along Γ/Z-S/R from the LCW-folded 2D-ACAR distribution measured in metallic sample $CM001$ [Fig. 7(e)]. Solid line: LCW applied on the anisotropic part of the 2D-ACAR (calculated on the minimum of the cylinders). Dotted line: LCW applied on the total 2D-ACAR. Long-dashed line: LCW applied on the isotropic part of the 2D-ACAR. The distributions are smoothed with a square function of 0.45 mrad side. Resolution FWHM: 0.5 mrad (with temperature broadening). The error bars are based on the statistic of the raw ACAR and of the efficiency function, and are shown for every third channel.

(generally 95%), the hypothesis suggesting that the observed set of points is described by the expected model. Some simulations were done giving an order of magnitude: let us take a step function of magnitude M, extended over 16 channels and altered by statistical noise of standard deviation σ. If M equals 4σ, the probability that the test will accept the hypothesis of a step signal within a confidence interval of 95% is one-half. If the expected model is unknown, the measured set of points may be compared with statistical noise, and the test decides if the points deviate from statistical noise. Such a test has been applied on a set of points lying in the line Γ/R-R/S, rejecting the presence of any structure within a confidence interval of 95%. The smooth modulation of the LCW structure is an argument which makes us cautious in interpreting our LCW results in terms of FS topology. Smedskjaer *et al.*[66] interpreted their LCW data differently, and discussions on the statistical interpretation are in progress.[66,67]

Another argument is that, even in the insulating phase, the general LCW distribution is similar to the metallic one. Despite the important difference between the measured 2D-ACAR spectra of the insulating and the metallic phases, their LCW-folded distributions [both for the (100) and (001) planes] look rather similar (left-hand and right-hand columns of Fig. 7): the wave-shaped oscillations in the LCW of $A110$ and $B110$ are reproduced in both phases within the statistical error; the LCW data of $C001$ also show similar features. The LCW theorem,[43] however, predicts a flat distribution for an insulating compound (fulfilling the conditions imposed by the theorem) when the momentum distribution is folded back into the first BZ. Exceptions arise when the positron carries momentum or if electrons are correlated (non-Fermi-liquid behavior[68]). In other insulating oxides, the study of LCW-folded data reveals varied behavior. In NiO, Wachs *et al.*[25] observe in their LCW data some deviations from the flat distribution, which they attribute to the momentum of the positrons in the crystal lattice. Tanigawa *et al.*[28,69] claim to see a FS in La_2CuO_4 in spite of a semiconductorlike resistivity behavior. Their argument is that transport properties are not directly connected to the electronic structure, but are dominated by scattering mechanisms.

Figure 9 shows the LCW spectra calculated in IPM and with the background subtracted following the same procedure as the one used experimentally. In the insulating case, the EMD should give a flat LCW distribution. Figure 9(d) shows the degree of numerical noise introduced by the use of a limited number of reciprocal-lattice vectors: the LCW distribution is not completely flat. In the Figs. 9(e) and 9(f) this numerical noise has been subtracted. It is encouraging to note that this correction improves the resemblance between our Fig. 9(e) and the corresponding one (Fig. 2) obtained by Singh *et al.*[23] Figure 9(f) extracted from the IPM-TPMD remains rather flat and shows only a small trend towards the dome obtained by experiment [Fig. 9(b)]. However, this could change somewhat if the $YBaCuO_6$ structure were correctly described and if enhancement were introduced. But no theory describing enhancement in insulators is yet available. In the metallic case, both EMD [Fig. 9(c)] and IPM-TPMD [Fig. 9(e)] LCW agree only roughly with the experiment [Fig. 9(a)]. In the calculations, the FS breaks are seen, even when the smoothing effect of twinning is taken into account.

The LCW structures are very sensitive to the positron behavior in the lattice. The FLAPW calculation provides a very reliable positron wave function in the interstitial region. In Fig. 10, the experimental LCW Γ/A-S/R line is compared with different calculations. The calculated lines are twinned and convoluted with experimental resolution. Figure 10(a) contains the experimental curve (solid line), our IPM LMTO calculation (dotted), and our FLAPW calculation (dashed) which includes the enhancement and the correlation potential for the positron. The LMTO calculation compared to FLAPW gives a somewhat different curve, due to a stronger step from the "barrel" bands. We note that our LMTO FS is in reasonable agreement with full potential calculations, but there is still room for improvement if the full-potential LMTO calculation is used (Andersen, private communication). The FLAPW IPM calculation by Singh *et al.*[23] is shown in Fig. 10(b) and the difference with our

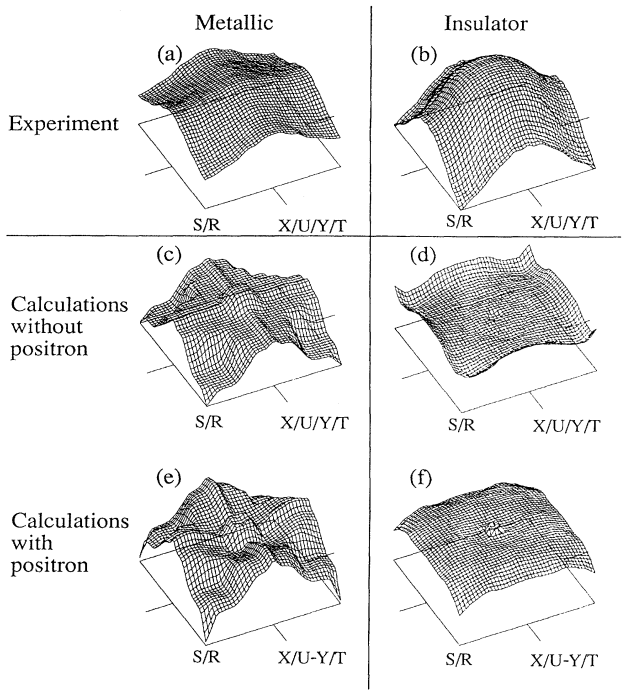

FIG. 9. (a) and (b) Experimental and (c)–(f) calculated LCW-folded distributions. First row: experimental LCW; second row: calculation without positron wave function; third row: calculation with positron wave function. (c) and (e) calculations with FS (at $E_F = 350$ mRy) in the $YBaCuO_7$ compound. (d) and (f) Calculations without FS in (d) $YBaCuO_7$ and in (f) $YBaCuO_6$ compounds. Only the nonconstant part of each distribution is shown after the subtraction of the same background for all distributions. In (c), (e), and (f) the numerical noise shown in (d) has been subtracted (see text). Vertical scales are identical. The calculated results are not convoluted with the experimental resolution function.

FLAPW are probably due to the enhancement factor for matrix elements.[51] Finally, in Fig. 10(c), we report the Bansil *et al.*[24] KKR IPM calculation which is in good agreement with FLAPW. In this calculation, the self-consistent band structure was obtained within the LMTO scheme and the resulting charge density was used to construct one-particle electron and positron muffin-tin potentials, which were the basis for computing TPMD using the KKR-based methodology.[70,71] In conclusion, all the calculations predict an important FS signal which should be detectable despite positron wave-function effects, but it is not observed by our measurements.

Several factors could contribute to the masking of the FS signal. The presence of a certain fraction of insulating phase in the metallic sample could be one reason. However, the sharp magnetic susceptibility transitions indicate isotropically distributed oxygens in the $YBa_2Cu_3O_{7-x}$ samples. The misalignment of the single-crystal mosaic, used in order to get a sufficient counting rate, could produce a broadening of the FS break, but recent measurements on one well-aligned single crystal do not produce significantly different results. Another factor could be positron trapping in defects, twin boundaries, and other phases of the material. FS broadening could also be produced by nonstoichiometric samples (disorder effect). At an oxygen concentration of 6.8 one has, on the average, one oxygen in every fifth of every unit cell missing. In many alloys, a rigid-band model works well, and nonstoichiometry can be described by band fillings and gives no large FS smearing. But the open structures of the oxide superconductors, with volatile oxygens, are different. Here, nonstoichiometry could induce local shifts of the potentials relative to E_F and also lead to strains in the structure, which all together may appear as a smeared FS. In an ideal case of a perfect sample, one may interpret the large broadening as coming from an intrinsic FS smoothing within the perfect crystal. This could come from an electron-electron correlation which predicts incomplete occupation of states below E_F and a tail of occupied states for higher energies. Such effects would be expected to become important near a Mott transition, and it is interesting to note the striking resemblance between our experimental LCW [Figs. 9(a) and 9(b)] and the momentum distribution of the 16×16 half-filled Hubbard lattice at $U=4$ as shown in Fig. 20 of Imada and Hatsuguai[68] (see also Baeriswyl and von der Linden[72]). In such a case, the non-Fermi-liquid behavior could itself describe the experimental LCW modulation even neglecting any positron effects. Finally, a small FS smearing of the LCW picture may also originate from the folding of high-momentum contributions. The reason is the small difference in x and y dimensions of the orthohombic cell ($\sim1.8\%$) which, for example, in the fifth zone of the twinned, tetragonal cell is amplified to 9%.

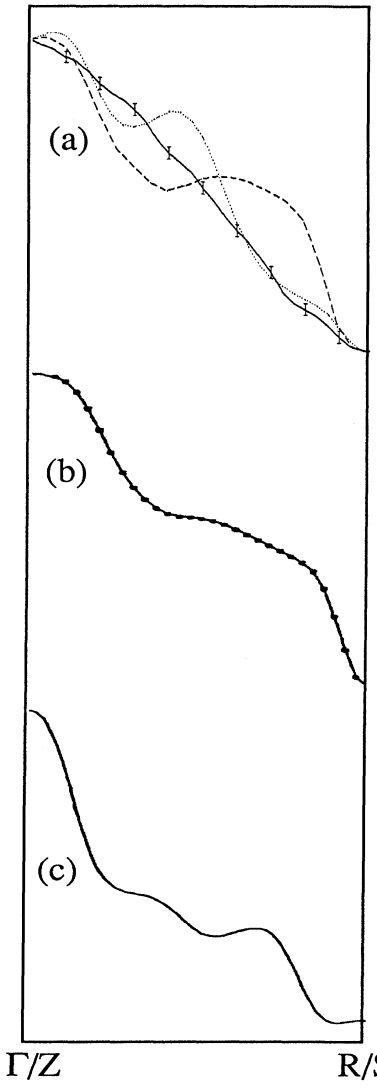

FIG. 10. Γ/Z-R/S lines extracted from the LCW-folded distributions. (a) Experimental (solid line), LMTO IPM [in contrast to Fig. 9(e), without noise subtraction] (dotted), and FLAPW with enhancement and positron correlation potential (dashed); (b) FLAPW according to Singh *et al.* (Ref. 23); (c) KKR according to Bansil *et al.* (Ref. 24).

In view of these difficulties encountered by the 2D-ACAR technique, it is interesting to review the results obtained by other methods. Campuzano *et al.*[73] using angular resolved photoemission spectroscopy (ARPES) interpret the intensity variations of their measurements as indications of **k** dispersions of distinct bands which disappear at E_F, similar to the LDA bands. The $Bi_2Sr_2CaCu_2O_8$ high-T_c superconductor has less volatile oxygens at the surface compared to $YBa_2Cu_3O_{7-x}$ and has been studied above and below T_c for an observation of the superconducting gap. A high-energy resolution of (angle-integrated) photoemission spectra has permitted Imer *et al.*[74] to identify the gap and to estimate a gap ratio $2\Delta/kT_c\sim8$. Angle-resolved high resolution by Olson *et al.*[75,76] shows strong temperature variations of the intensities when the bands approach E_F and they deduce from this a gap ratio of about 7. The electron-energy-loss-spectroscopy (EELS) measurements[77,78] probe the nonoccupied states. Measurements[77] on $La_{2-x}Sr_xCuO_4$

are taken as evidence for the formation of a charge-transfer gap[79,80] at small doping x, not described by LDA theory. In ACAR, we have included matrix elements and even estimated enhancement effects, as opposed to ARPES. Matrix element effects, which depend on the symmetry of initial and final states as well as on **k** conservation, are important in ARPES. Also in EELS, matrix elements and core-hole relaxations may be important for interpretation. Therefore, there may be surprises when the spectroscopic data are faced with a more careful analysis of LDA bands. In spite of this note of caution (due to rapid interpretation of spectroscopic data), it is important to remark that these data contain clear structures. This makes a discussion possible, while in ACAR data there are almost no visible structures when sufficient statistics are collected. In view of this, we are obliged to conclude something similar to von Stetten and Berko,[67] namely, it is important to await better statistics and optimal samples. Only then can one confirm or disclaim the existence of a FS.[73–76,81,82]

E. Superconducting transition

How do positrons interact with a superconducting gap (assuming there is one)? We may consider two independent effects: First, the loss of the initial kinetic energy of positrons may be incomplete,[83] inducing a change of the positron minimal energies between the normal and the superconducting states. Second, the Fermi break in momentum space, according to BCS theory, is smoothed due to the redistribution of the electronic states.[84] Many Doppler-broadening results in metallic $YBa_2Cu_3O_{7-x}$ presenting anomalies, at temperatures comparable T_c, were interpreted as a change of the electronic densities due to the superconducting transition.[13–15] It has also been observed[85] that they are not modified by a magnetic field of 4.5T. In 1969, 1D-ACAR measurements[86] on Nb_3Sn at different temperatures were presented showing an anomaly at the Fermi momentum reflecting the redistribution of the electronic states. However, our 2D-ACAR measurement (with two times better angular resolution) on Nb_3Sn did not show this anomaly.[63]

What should we expect in $YBa_2Cu_3O_{7-x}$? Since the coherence length ξ of the superconducting electrons is about 5 Å in the **c** direction (ten times smaller than in Nb_3Sn), the induced gap $\delta\mathbf{k}$ in momentum space (inverted coherence length) is about 0.5 mrad [$\delta\mathbf{k}=2/(\pi/\xi)$] for $T=0$ as shown by Barnes and Peter,[84] and for temperatures around T_c,[87]

$$\delta\mathbf{k}=2/[\pi/\xi)_x 4kT_c/(2\Delta_0)] ,$$

which is comparable to the experimental resolution.

We have measured below (77 K) and above T_c (97 K), a sample provided by Damento *et al.*[33] ($T_c \sim 87$ K). We have integrated along the $(\bar{1}10)$ component the difference between the normalized 2D-ACAR's measured above and below T_c. We were not able to identify any structure corresponding to the superconducting transition, with an amplitude greater than the statistical error. The result is a smooth modulation, negative around zero momentum and positive for higher momenta, exhibiting the narrowing of the spectrum measured at 97 K. This contradicts the conclusions of Liu *et al.*,[88] who fit their Doppler-broadening data with a theoretical curve based on Cooper-pair formation. Concerning the c plane, the coherence length is three times larger, and $\delta\mathbf{k}$ is about 0.2 mrad (below the angular resolution). On comparing the c-plane-measured LCW of Haghighi *et al.*[57] at room temperature with ours at 40 K, no striking differences appear.

IV. CONCLUSION AND OUTLOOK

The work reported here was undertaken with the hope of identifying FS sheets with clarity and resolution comparable to results obtained previously in metals and compounds, and to establish correspondence between the measured TPMD and predictions obtained from band-structure calculations. In addition, we had some hope of discovering characteristic modifications of the TPMD above and below T_c with the possibility of deriving some hints about the fundamental mechanism of superconductivity in the oxides, as exemplified by the 123 compound. Other specific properties such as the presumably important magnetic fluctuation behavior,[89] seem to be inaccessible to our technique.

Our very extensive measurements on samples from different sources did not, however, give us clear evidence for FS, or for temperature effects at T_c. On the other hand, TPMD resembles band-structure predictions (even though a numerical study in the t-J model[68] proposes a histogram which also resembles experiment).

The relatively poor agreement between theoretical expectations and experiment forces us to examine the question of the quality of the experiment from the point of view of samples, measurement and evaluation. The evidence presented allows one to judge the degree of precautions taken in our experiments. Much work was invested in the growth of large single-crystals and in the verification of their properties (see Sec. II A). Samples of both the $YBaCuO_6$ and $YBaCuO_7$ variety were produced, and in the case of one sample, oxidation could be changed reversibly. The observation of both metallic and insulating samples alerted us to the fact that a direct interpretation of the experimental data in terms of FS topology (adequate in the case of many metals), is not admissible in these oxides.

The experimental data were collected with very high statistics. Factors such as alignment and influence of twinning were discussed. They may diminish the sharpness of the effects we are looking for, but not to the extent of explaining their absence. A large unknown is the influence of imperfections, and of the fractional oxygen valence, on the state of electrons and positrons. The possibility of localization in a partially random lattice cannot be excluded. If this localization occurs in the chains, it might prevent us from seeing FS effects.

Lifetime measurements give information on the question of localization. In view of the difficulty in the interpretation of lifetime spectra containing several species, we hesitate to interpret these results as excluding locali-

zation effects. There exist experimental and theoretical investigations of the temperature dependence of the signal of trapped positrons[90] in metals which suggest that a study of ACAR over larger temperature ranges might shed some light on the influence of imperfections. It would be helpful to know whether such imperfections contribute also to the anisotropic part of TPMD.

A comparison of the observed TPMD projections with predictions from band theory calls for a critical evaluation of available band-structure results, both in full and in reduced momentum space (LCW folding). In full space, the features of the participating atomic functions are brought out. The extent of this domination of the atomic structure over FS effects is illustrated by the success of the MO-LCAO method[25,26] which amounts to using a full band of MO wave functions, even in the metallic samples. The effects of partial filling are neglected because they are small with respect to the multitude of filled bands. The smallness of the effect of unfilled bands is also used to estimate the TPMD in the insulating compound from LDA calculations which, strictly speaking, also produce a metallic state in the $YBaCuO_6$ compound. Coincidence between the calculated results and our measurements is not very good, but the agreement has been improved by including enhancement effects[50] and correlation positron potential.[49] We interpret this improvement as an observation of correlation effects by ACAR in oxides.

LCW folding produces, in the case of IPM and a constant positron wave function, a distribution of occupation numbers in the reduced BZ ($\mathbf{k}$ space). For full bands, this should be just a constant, and so LCW should not be used in MO-LCAO. The calculation predicts FS-related features, mainly due to chain-related band crossings and much less due to the planes because of the density distribution of the positrons. We do not believe that our experimental data have reproduced these features which should have appeared with a comfortable signal-to-noise ratio in our statistics. We think that, in spite of this evidence, it may be premature to conclude that Fermi breaks are intrinsically absent. We have pointed out previously that our measurements on different samples gave different intensities both in the isotropic and in the anisotropic part, as well as in the metallic-insulating ratios. This means that sample preparation remains a crucial factor. Furthermore, the results of ARPES in the same compound show us bandlike features which become unoccupied as the energy increases.[73] The transition between the full and the empty part may be associated with E_F. However, the width of this transition (due to electron correlation) may be considerable in view of the resolution which is still modest compared to the relevant energy scale. It must, however, be admitted that the recent ARPES data of Olson *et al.*[75] have even shown the effect of superconductivity on these bandlike features. So it seems reasonable to admit that, on a certain scale of resolution of momentum and energy, a band model should apply, and that the question raised by our experiments is why do we not see this structure. We have reviewed a certain number of possible answers, to which we might add that our method is bulk-sensitive while ARPES (Ref. 75) and EELS (Ref. 78) reveal mostly surface properties. The question of whether the observed bandlike features are split in these oxides, by Hubbard terms, is still open.[91] ACAR data might help to decide this question.

We believe that our results point to the need for stronger, well-focused beams, better detectors, progress in sample preparation and characterization, study of several different high-T_c oxides besides $YBaCuO_7$, and better theoretical prediction of the expected features leading to optimal statistical planning and evaluation of experiments.

ACKNOWLEDGMENTS

It is a pleasure to thank P.-E. Bisson for his technical assistance during the measurements, G. Triscone for the Meissner-effect measurements, and P. Bouvier for measuring superconducting transition temperatures. The active support of P. Moser during the assembling of the lifetime spectrometer was greatly appreciated. We are grateful to O. K. Andersen, A. Baldereschi, A. Bansil, T. Chiba, R. H. Howell, K. G. Lynn, M. Schlueter, L. C. Smedskjaer and S. Tanigawa for stimulating discussions. Finally, we thank H. R. Ott, W. B. Waeber, and U. Zimmermann for their active interest in the positron annihilation field. This work was supported by the Fonds National Suisse de la Recherche Scientifique under Grant Nos. 2.029-0.86 and 2.426-0.87.

[1] J. G. Bednorz and K. A. Müller, Z. Phys. B **64**, 189 (1986).

[2] B. Raveau, C. Michel, M. Hervieu, and J. Provost, Proceedings of the International Conference on High Temperature Superconductors and Materials and Mechanisms of Superconductivity Held in Interlaken, 1988, [Physica C **153-155**, 3 (1988)].

[3] A. W. Sleight, Proceedings of the International Conference on High Temperature Superconductors and Materials and Mechanisms of Superconductivity Held in Stanford, 1989, [Physica C **162-164**, 3 (1989)].

[4] A. A. Manuel, J. Phys. Condens. Matter **1**, SA107 (1989).

[5] S. Ishibaski, Y. Suzuki, R. Yamamoto, T. Hatano, K. Ogawa, and M. Doyama, Phys. Lett. A **128**, 387 (1988).

[6] P. Moser and J. Y. Henry, in *Positron Annihilation*, edited by L. Dorikens-Vanpraet, M. Dorikens, and D. Segers (World-Scientific, Singapore, 1988), p. 904.

[7] C. S. Sundar, A. K. Sood, A. Bharathi, and Y. Hariharan, Pramana **30/2**, L161 (1988); Physica C **153-155**, 155 (1988).

[8] C. Corbel, P. Bernède, H. Pascard, F. Rullier-Albenque, R. Korman, and J. F. Marucco, Appl. Phys. A **48**, 335 (1989).

[9] D. R. Harshman, L. F. Schneemeyer, J. V. Waszczak, Y. C. Jean, M. J. Fluss, R. H. Howell, and A. L. Wachs, Phys. Rev. B **38**, 848 (1988).

[10] Y. C. Jean, J. Kyle, H. Nakanishi, P. E. A. Turchi, R. A. Howell, A. L. Wachs, M. J. Fluss, R. L. Meng, H. P. Hor, J. Z. Huang, and C. W. Chu, Phys. Rev. Lett. **60**, 1069 (1988).

[11] Y. C. Jean, C. S. Sundar, A. Bharathi, J. Kyle, H. Nakanishi, P. K. Tseng, P. H. Hor, R. L. Meng, J. Z. Huang, C. W. Chu, Z. Z. Wang, P. E. A. Turchi, R. A. Howell, A. L. Wachs, and M. J. Fluss, Phys. Rev. Lett. **64**, 1593 (1990).

[12] C. S. Sundar, A. Bharathi, L. Hao, Y.C. Jean, P. H. Hor, R. L.

Meng, Z.J. Huang, and C. W. Chu (unpublished).
[13]S. Ishibashi, A. Yamaguchi, Y. Suzuki, M. Doyama, H. Kumakura, and K. Togano, Jpn. J. Appl. Phys. **26**, L688 (1987).
[14]Y. C. Jean, S. J. Wang, H. Nakanishi, W. N. Hardy, M. E. Hayden, R. F. Keifl, R. L. Meng, H. P. Hor, J. Z. Huang, and C. W. Chu, Phys. Rev. B **36**, 3994 (1987).
[15]S. G. Usmar, P. Sferlazzo, K. G. Lynn, and A. R. Moodenbaugh, Phys. Rev. B **36**, 8854 (1987).
[16]E. C. von Stetten, S. Berko, X. S. Li, J. Brynestad, D. Singh, H. Krakauer, W. E. Pickett, and R. E. Cohen, Phys. Rev. Lett. **60**, 2198 (1988).
[17]S. Berko, in *Positron Solid-State Physics,* edited by W. Brandt and A. Dupasquier (North-Holland, Amsterdam, 1983).
[18]P. E. Mijnarends, in *Positrons in Solids,* edited by P. Hautojarvi (Springer-Verlag, New York, 1979), p. 25.
[19]T. Jarlborg, and G. J. Arbman, J. Phys. F **6**, 189 (1976).
[20]T. Jarlborg, A. A. Manuel, and M. Peter, Phys. Rev. B **27**, 4210 (1983).
[21]T. Jarlborg, M. Peter, and W. Weber, J. Phys. F **17/4**, 913 (1987).
[22]S. Massidda, Physica C **169**, 137 (1990).
[23]D. Singh, W. E. Pickett, E. C. von Stetten, and S. Berko, Phys. Rev. B **42**, 2696 (1990).
[24]A. Bansil, P. E. Mijnarends, and L. C. Smedskjaer, Bull Am. Soc. **35**, 427 (1990).
[25]A. L. Wachs, P. E. A. Turchi, Y. C. Jean, K. H. Wetzler, R. H. Howell, M. J. Fluss, D. R. Harshman, J. P. Remieka, A. S. Cooper, and R. M. Fleming, Phys. Rev. B **38**, 913 (1988).
[26]P. E. A. Turchi, A. L. Wachs, Y. C. Jean, R. H. Howell, K. H. Wetzler, and M. J. Fluss, Physica C **153-155**, 157 (1988).
[27]T. Chiba, J. Chem. Phys. **64**, 1182 (1976).
[28]S. Tanigawa, Y. Mizuhara, Y. Hidaka, M. Oda, M. Suzuki, and T. Murakami, Mater. Res. Soc. **5**, 57 (1988).
[29]L. C. Smedskjaer, J. Z. Liu, R. Benedek, D. G. Legnini, D. J. Lam, M. D. Stahulak, and H. Claus, Physica C **156**, 269 (1988).
[30]A. Bansil, R. Pankaluoto, R. S. Rao, P. E. Mijnarends, W. Dlugosz, R. Prasad, and L.C. Smedskjaer, Phys. Rev. Lett. **61**, 2480 (1988).
[31]M. Peter, L. Hoffmann, and A. A. Manuel, Physica C **153-155**, 1724 (1988).
[32]M. Peter and A. A. Manuel, Phys. Scr. **T29**, 106 (1989).
[33]M. A. Damento, K. A. Gschneider, and R. W. McCallum, Appl. Phys. Lett. **51**, 690 (1987).
[34]L. Hoffmann, A. A. Manuel, M. Peter, E. Walker, and M. A. Damento, Europhys. Lett. **6**, 61 (1988).
[35]L. Hoffmann, A. A. Manuel, M. Peter, E. Walker, and M. A. Damento, Physica C **153-155**, 129 (1988).
[36]M. Peter, L. Hoffmann, and A. A. Manuel, in *Positron Annihilation,* edited by L. Dorikens-Vanpraet, M. Dorikens, and D. Segers (World-Scientific, Singapore, 1988), p. 197.
[37]M. Peter, IBM J. Res. Dev. **33**, 333 (1988).
[38]W. Sadowksi and H. J. Scheel, J. Less Common Met. **150**, 219 (1989).
[39]J. Rossat-Mignod, P. Burlet, M. J. Jurgens, C. Vettier, L. P. Regnault, J. Y. Henry, C. Ayache, L. Forro, H. Noel, M. Potel, P. Gougeon, and J. C. Levet, J. Phys. (Paris) Colloq. **49**, C8-2119 (1988).
[40]P. E. Bisson, P. Descouts, A. Dupanloup, A. A. Manuel, E. Perreard, M. Peter, and R. Sachot, Helv. Phys. Acta **55**, 100 (1982).
[41]M. O. Bedwell, and T. J. Paulus, in *Positron Annihilation,* edited by R. R. Hasiguti and K. Fujiwara (Japan Institute of Metals, Japan, 1979), p. 375.
[42]P. Kirkegaard, M. Eldrup, O. E. Mogensen, and N. J. Pederson, Comput. Phys. Commun. **23**, 307 (1981).
[43]D. G. Lock, V. H. C. Crisp, and R. N. J. West, Phys. F **3**, 561 (1973).
[44]L. Hoffmann, P. Genoud, T. Jarlborg, A. A. Manuel, M. Peter, W. Sadowski, and A. K. Singh, in *Positron Annihilation and Compton Scattering,* edited by B. K. Sharma, P. C. Jain, and R. M. Singru (Omega Scientific Publishers, New Delhi, 1990), p. 221.
[45]T. Jarlborg, A. A. Manuel, M. Peter, and A. K. Singh, in *Positron Annihilation,* edited by L. Dorikens-Vanpraet, M. Dorikens, and D. Segers (World-Scientific, Singapore, 1988), p. 898.
[46]T. Jarlborg, Solid State Commun. **67**, 297 (1988).
[47]S. Massidda, J. Yu, A. J. Freeman, and D. D. Koelling, Phys. Lett. A **122**, 198 (1987).
[48]J. Yu, S. Massidda, A. J. Freeman, and D. D. Koelling, Phys. Lett. A **122**, 203 (1987).
[49]E. Boronski, and R. M. Nieminen, Phys. Rev. B **34**, 3820 (1986).
[50]A. K. Singh and T. Jarlborg, J. Phys. F **15**, 727 (1985).
[51]T. Jarlborg and A. K. Singh, Phys. Rev. B **36**, 4660 (1987).
[52]A. Bharathi, C. S. Sundar, and Y. Hariharan, J. Phys. Condens. Matter **1**, 1467 (1989).
[53]K. O. Jensen, R. M. Nieminen, and M. J. Puska, J. Phys. Condens. Matter **1**, 3727 (1989).
[54]D. Singh, W. E. Pickett, R. E. Cohen, H. Krakauer, and S. Berko, Phys. Rev. B **39**, 9667 (1989).
[55]S. Daniuk, G. Kontrym-Sznajd, J. Majsnerowski, M. Sob, and H. Stachowiak, J. Phys. Condens. Matter **1**, 6321 (1989).
[56]H. Sormann, Phys. Status Solidi B **142**, K45 (1987).
[57]H. Haghighi, J. H. Kaiser, S. Rayner, R. N. West, M. J. Fluss, R. H. Howel, P. E. A. Turchi, A. L. Wachs, Y. C. Jean, and Z. Z. Wang, J. Phys. Condens. Matter **2**, 1911 (1990).
[58]E. C. von Stetten, S. Berko, X. S. Li, L. F. Schneemeyer, J. Brynestad, D. Singh, H. Krakauer, W. E. Pickett, and R. E. Cohen, in *Positron Annihilation,* edited by L. Dorikens-Vanpraet, M. Dorikens, and D. Segers (World-Scientific, Singapore, 1988), p. 913.
[59]R. N. West, A. Alam, P. A. Walters, J. D. McGervey, in *Positron Annihilation,* edited by P. G. Coleman, S. C. Sharma, and L. M. Diana (North-Holland, Amsterdam, 1982), p. 337.
[60]A. Alam, J. H. Kaiser, P. A. Walters, R. L. Waspe, and R. N. West, in *Positron Annihilation,* edited by P. G. Coleman, S. C. Sharma, and L. M. Diana (North-Holland, Amsterdam, 1982), p. 337.
[61]L. Hoffmann, T. Jarlborg, A. A. Manuel, M. Peter, A. K. Singh, E. Walker, M. Weger, and A. Simievic, Physica B+C **135**, 350 (1985).
[62]L. Hoffman, A. K. Singh, H. Takei, and N. Toyota, J. Phys. **18**, 2605 (1988).
[63]L. Hoffmann, Ph.D. thesis, University of Geneva, 1989.
[64]S. Tanigawa (unpublished).
[65]I. N. Gibra, in *Probability and Statistical Inference for Scientists and Engineers* (Prentice-Hall, Englewood Cliffs, New Jersey, 1973).
[66]L. C. Smedskjaer, A. Bansil, and P. E. Mijnarends, Phys. Rev. Lett. **65**, 136 (1990).
[67]E. C. von Stetten and S. Berko, Phys. Rev. Lett. **65**, 135 (1990).
[68]M. Imada and Y. Hatsugai, J. Phys. Soc. Jpn. **58**, 3752 (1989).
[69]S. Tanigawa, Y. Mizuhara, T. Kurihara, M. Osawa, Y. Hidaka, M. Oda, Y. Enomoto, M. Suzuki, and T. Murakami, in *Positron Annihilation,* edited by L. Dorikens-Vanpraet, M.

Dorikens, and D. Segers (World-Scientific, Singapore, 1988), p. 933.
[70]P. E. Mijnarends and A. Bansil, Phys. Rev. B **13**, 2381 (1976).
[71]P. E. Mijnarends and L. P. L. M. Rabou, J. Phys. F **16**, 483 (1986).
[72]D. Baeriswyl and W. von der Linden, J. Mod. Phys. B (to be published).
[73]J. C. Campuzano, G. Jennings, M. Faiz, L. Beaulaigue, B. W. Veal, J. Z. Liu, A. P. Paulikas, K. Vandervoort, H. Claus, R. S. List, A. J. Arko, and R. J. Bartlett, Phys. Rev. Lett **64**, 2308 (1990).
[74]J.-M Imer, F. Patthey, B. Dardel, W.-D. Schneider, Y. Baer, Y. Petroff, and A. Zettl, Phys. Rev. Lett. **62**, 336 (1989).
[75]C. G. Olson, R. Liu, A.-B. Yang, D. W. Lynch, A. J. Arko, R. S. List, B. W. Veal, Y. C. Chang, P. Z. Ziang, and A. P. Paulikas, Science **245**, 731 (1989).
[76]C. G. Olson, R. Liu, D. W. Lynch, R. S. List, A. J. Arko, B. W. Veal, Y. C. Chang, P. Z. Jiang, and A. P. Paulikas, Phys. Rev. B **42**, 381 (1990).
[77]H. Romberg, M. Alexander, N. Nücker, P. Adelmann, and J. Fink, Phys. Rev. B **42**, 8768 (1990).
[78]R. C. Claessen, G. Mante, A. Huss, R. Manzke, M. Sibowksi, T. Wolf, and J. Fink (unpublished).
[79]J. Zaanen, G. A. Sawatzky, and J. W. Allen, Phys. Rev. Lett. **55**, 418 (1985).
[80]H. Eschrig, Physica C **159**, 545 (1989).
[81]R. S. List, A. J. Arko, T. Fisk, S. W. Cheong, S. D. Conradson, J. D. Thompson, C. B. Pierce, D. E. Peterson, R. J. Bartlett, J. A. O'Rourke, N. D. Shinn, J. E. Schirber, C. G. Olson, A. B. Yang, T. W. Pi, B. W. Veal, A. P. Paulikas, and J. C. Campuzano, in *High-T_c Superconducting Thin Films, Devices, and Applications,* Proceedings of the 1988 topical conference on High-T_c Superconducting Thin Films, Devices, and Applications of the AVS held in Atlanta, GA, October 1988, AIP Conf. Proc. No. 182, edited by Giorgio Magaritondo, Robert Joynt, and Marshall Onellion (AIP, New York, 1989).
[82]R. S. List *et al.*, J. Appl. Phys. (to be published).
[83]A. Perkins and E. J. Woll, Phys. Rev. **178**, 530 (1969).
[84]S. E. Barnes and M. Peter, Phys. Rev. B **40**, 10 958 (1989).
[85]R. S. Brusa, A. Dupasquire, R. Grisenti, S. Liu, S. Oss, and A. Zecca, in *Positron Annihilation,* edited by L. Dorikens-Vanpraet, M. Dorikens, and D. Segers (World-Scientific, Singapore, 1988), p. 907.
[86]G. Faraci and M. Spadoni, Phys. Rev. Lett. **22**, 928 (1969).
[87]B. L. Gyorffy, Z. Szotek, W. M. Temmerman, and G. M. Stocks, J. Phys. Condens. Matter **1**, SA119 (1989).
[88]S. H. Liu, W. F. Huang, Z. J. Xu, and M. K. Wu (unpublished).
[89]T. Moriya, Tech. Rep. JSSP Ser. **A9**, 2267 (1990).
[90]A. Seeger and F. Banhart, Helv. Phys. Acta **63**, 403 (1990).
[91]C. T. Chen, F. Sette, Y. Ma, M. S. Hybertsen, E. B. Stechel, W. M. C. Foulkes, M. Schluter, S-W. Cheong, A. S. Cooper, L. W. Rupp, Jr., B. Batlogg, Y. L. Soo, Z. H. Ming, A. Krol, and Y. H. Kao, Phys. Rev. Lett. **66**, 104 (1991).